Alongshelf Variability of Inner-Shelf Circulation along the Central Oregon Coast during Summer

ANTHONY R. KIRINCICH* AND JOHN A. BARTH

College of Oceanic and Atmospheric Sciences, Oregon State University, Corvallis, Oregon

(Manuscript received 11 January 2007, in final form 17 October 2008)

ABSTRACT

The spatial and temporal variability of inner-shelf circulation along the central Oregon coast during the 2004 upwelling season is described using a 70-km-long array of moorings along the 15-m isobath. Circulation at three stations located onshore of a submarine bank differed from that of a station north of the bank, despite the relatively uniform wind forcing and inner-shelf bathymetry present. During upwelling-favorable winds, strong southward alongshelf flow occurred north of the bank, no alongshelf flow occurred onshore of the northern part of the bank, and increasing southward flow occurred onshore of the southern part of the bank. During downwelling-favorable winds, strong northward flow occurred in the inner shelf onshore of the bank while weak flow occurred north of the bank. These alongshelf differences in inner-shelf circulation were due to the effects of the bank, which isolated the inner shelf onshore of the bank from the regional upwelling circulation that was evident at the northernmost station. As a result, circulation onshore of the bank was driven primarily by local wind forcing, while flow north of the bank was only partially driven by local winds. A secondary mode of variability, attributed to the movement of the regional upwelling jet due to remote forcings, contributed the bulk of the variability observed north of the bank. With the time-dependent wind forcing present, acceleration was an important term in the depth-averaged alongshelf momentum equation at all stations. During upwelling, bottom stress and acceleration opposed the wind stress north of the bank, while bottom stress was weaker onshore of the bank where the across-shelf momentum flux and the alongshelf pressure gradient balanced the residual of the acceleration and stresses. During downwelling, waters onshore of the bank surged northward at magnitudes much larger than that found north of the bank. These spatial variations developed as the season progressed and the regional upwelling circulation intensified, explaining known variations in growth and recruitment of nearshore invertebrate species.

1. Introduction

The inner shelf of the central Oregon coast has recently been the focus of an intensive monitoring effort by the Partnership for Interdisciplinary Studies of Coastal Oceans (PISCO) program. Observations from the PISCO seasonal array of moorings have allowed us to extend our knowledge of the Oregon upwelling system into the inner shelf, a previously poorly resolved area of the coastal ocean off Oregon. A recent work by Kirincich et al. (2005) used four years of PISCO observations to quantify the across-shelf divergence of Ekman transport that marks the region of active upwelling: finding that the measured across-shelf surface transport was 25% of the full theoretical Ekman transport in 15 m of water, 1–2 km offshore, and 100% of full Ekman transport in 50 m of water, 5–6 km offshore. Thus this divergence, which defines the inner shelf and controls across-shelf access of water masses, nutrients, and planktonic larvae between the surf zone and the coastal ocean, was limited to a narrow area adjacent to the coast. The present study describes spatial variations of inner-shelf circulation at these same stations. Using PISCO observations of velocity, bottom pressure, and hydrography, we analyze inner-shelf upwelling and downwelling dynamics, and put the alongshelf variations measured in the context of both the known local shelf-wide circulation and the known inner-shelf dynamics.

Offshore of the inner shelf, oceanic conditions along the central Oregon coast have been investigated in numerous process studies and long-term monitoring projects, which together provide a description of circulation over the

* Current affiliation: Woods Hole Oceanographic Institute, Woods Hole, Massachusetts.

Corresponding author address: Anthony R. Kirincich, Woods Hole Oceanographic Institute, Woods Hole, MA 02543.
E-mail: akirincich@whoi.edu

DOI: 10.1175/2008JPO3760.1

middle and outer shelves. During summer, the region is forced by intermittent upwelling favorable winds (Smith 1974; Huyer et al. 1974). Nearly spatially uniform with minimal wind stress curl (Samelson et al. 2002; Kirincich et al. 2005), these winds push the Columbia River plume, the only significant source of freshwater to the region during summer, offshore soon after upwelling begins (Huyer 1983). North of Newport, Oregon, in a region of simple shelf topography, upwelling circulation is essentially two-dimensional (2D) with little variation in the alongshelf direction (Kundu and Allen 1976). Here, in water depths of 100 m, both observations and model studies report geostrophy as the primary balance in the depth-averaged alongshelf momentum equation (Allen and Smith 1981; Oke et al. 2002). A secondary balance between the alongshelf wind and bottom stresses existed, closed by acceleration at periods less than 10 days and the barotropic pressure gradient at longer periods. Additional work (Federiuk and Allen 1995; Lentz and Chapman 2004) has shown that nonlinear terms, specifically the across-shelf momentum flux, can be substantial on the Oregon shelf, balancing the wind stress during upwelling. Yet onshore, at depths of 50 m, the classic 2D balance (Allen and Smith 1981) of wind stress, bottom stress, and acceleration appears to dominate the alongshelf momentum balance during upwelling events (Oke et al. 2002). Variations in alongshelf currents along the Oregon coast have been linked to the northward propagation of both free and forced coastal trapped waves (CTWs) (Cutchin and Smith 1973; Battisti and Hickey 1984). Around Newport, a three-dimensional (3D) circulation pattern develops as the southward flowing upwelling jet encounters an offshore submarine bank (the Heceta and Stonewall Bank complex, Fig. 1). As the season progresses, the jet is forced offshore and around the western edge of the bank, creating a ''lee'' region over the bank (Castelao and Barth 2005; Oke et al. 2002; Kosro 2005). Localized coastal upwelling has been reported onshore of the bank (Kosro 2005; Barth et al. 2005b).

Inner-shelf circulation along the central Oregon coast has not been investigated on the spatial and temporal scales of these outer-shelf studies, and physical conditions in the inner-shelf contrast with those found offshore. Forced by the same predominantly alongshelf uniform winds as offshore, inner-shelf bathymetry at depths less than 50 m is predominantly alongshelf-uniform, in contrast to that found offshore. As a result, the across-shelf scale of the divergence of Ekman transport has no alongshelf trends in this region (Kirincich et al. 2005). Yet, the growth (Menge et al. 2002) and recruitment (Barth et al. 2007) of intertidal invertebrate species onshore of the bank were consistently higher than at sites to the north or south. Nutrients and primary production had similar patterns (Leslie et al. 2005). It has been suggested that oceanographic processes distinct to the inner shelf could be the primary driver for these variations.

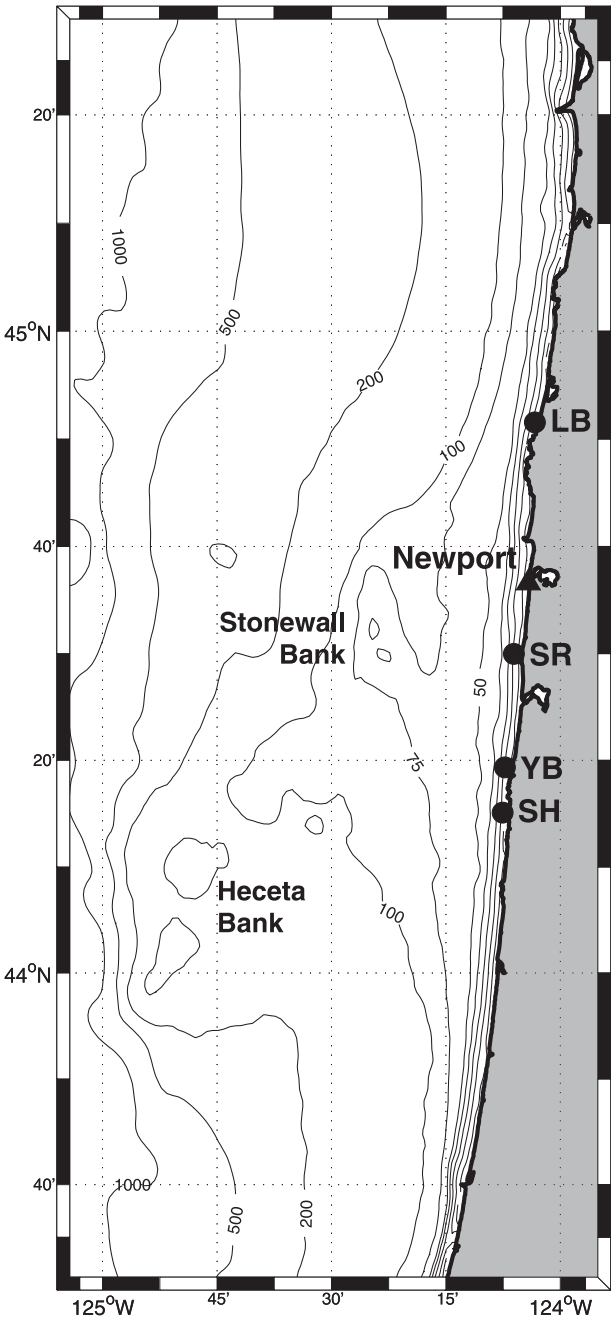

FIG. 1. The central Oregon shelf: The Heceta and Stonewall Bank complex is shown by bathymetric contours offshore of the 50-m isobath and south of 44°45′ latitude. Locations of the four PISCO stations (bullets) and the Newport CMAN station (triangle) are shown. Bathymetry is in meters and in 10-m increments onshore of the 50-m isobath.

In other regions, inner-shelf studies have described the transition of shelf-scale circulation into the surf zone

inshore, both in coastal regions influenced by buoyant plumes (Wiseman and Garvine 1995; Yankovsky et al. 2000; Munchow and Chant 2000; Codiga 2005) and on predominantly wind-driven shelves (Lentz and Winant 1986; Lentz 1994; Lentz et al. 1999; Liu and Weisberg 2005). For wind-driven shelves similar to the Oregon coast, inner-shelf circulation is dominated by alongshelf currents closely linked to large-scale wind stress and pressure gradients but with magnitudes that are reduced relative to the outer shelf (Lentz 1994). Along the outer edge of the surf zone, depth-averaged momentum balances are dominated by the surface and bottom stresses in the alongshelf direction and wave setup in the across-shelf direction (Lentz et al. 1999). Offshore, geostrophy dominates the across-shelf momentum balance, while a complex combination of surface and bottom stresses, pressure gradients, and acceleration exists in the alongshelf direction (Lentz et al. 1999; Liu and Weisberg 2005). However, numerical modeling studies of the inner shelf (Austin and Lentz 2002; Kuebel Cervantes et al. 2003; Tilburg 2003) have illustrated the variations on this general description caused by the movement of density stratification during upwelling or downwelling events. Additionally, alongshelf variations of inner-shelf bathymetry or forcing conditions lead to alongshelf variations in the circulation patterns described (Yankovsky and Chapman 1995; Tilburg and Garvine 2003).

Given the contrast of nearly uniform bathymetry and wind forcing near the coast and nonuniform bathymetry and circulation offshore, it is not known how circulation along the central Oregon inner-shelf compares with that found offshore. Thus, this paper intends to document the physical characteristics and alongshelf variations of circulation on the central Oregon inner shelf. Focusing on the observations made by PISCO during the 2004 upwelling season provides a compact way to accomplish this, as forcing conditions were typical of those usually observed along the central Oregon coast (Pierce et al. 2006). Yet, it should be noted that, while the placement of the moored array and its instruments was not designed for a complete dynamical analysis at each station, the available data do enable an estimation of the terms in the alongshelf momentum equation. Data sources and processing steps are described first (section 2), followed by a general description of inner-shelf circulation in the region (section 3), an analysis of the modes of variability present using empirical orthogonal functions (section 4), and a dynamical description of circulation using the depth-averaged alongshelf momentum balance (section 5). We then discuss these results in the context of the known regional circulation and its ecological variations (section 6) before concluding (section 7).

2. Data sources

During the summer of 2004, PISCO maintained moorings at four inner-shelf stations along a 67-km stretch of the Oregon coast centered around Newport, Oregon (Fig. 1; Table 1). These stations, listed from north to south as Lincoln Beach (LB), Seal Rock (SR), Yachats Beach (YB), and Strawberry Hill (SH), were each located along the 15-m isobath approximately 1 km offshore. The northernmost station, LB, was located in a region of simple shelfwide topography, while SR, YB, and SH were located onshore of the Stonewall and Heceta Bank complex. For simplicity we refer to LB, located off the north end of the bank, as the ''off bank'' station, and the southern three stations, located onshore of the bank, as the ''on bank'' stations.

At each station, a bottom-mounted upward-looking acoustic Doppler current profiler (ADCP) was deployed along with a mooring of temperature and conductivity sensors (Table 1). The ADCP, an RD Instruments (RDI)Workhorse 600-kHz model, collected ensemble averages of velocity profiles in 1-m depth bins between 2.5 m above the bottom and 1 m below the surface. Bottom pressure was recorded by the ADCP using a Keller 5-Bar, sealed-gauge, piezoresistive pressure transducer. ADCP velocities, composed of 2-min ensemble averages of 40 pings separated by 1.5 s, have estimated uncertainties of 0.01 m s^{-1} (Gordon 1996). Pressure sensor accuracies were estimated using paired at-sea vertical casts, yielding rms differences of 1 mbar with a standard error for the differences of 0.125 mbar. The hydrographic moorings measured temperature at 1, 4, 9, and 14 m with Onset XTI or Tidbit loggers and temperature and conductivity at 8- or 11-m depth using Seabird 16 or 37 recorders (Table 1). Sample rates varied from 2 to 10 min for these sensors and measurement uncertainty varied from 0.2°C for Onset temperature loggers to 0.005°C and 0.0005 S m^{-1} for Seabird temperature and conductivity sensors.

From these measurements, we derived hourly averaged time series of alongshelf velocity, across-shelf surface transport, pressure anomaly, and density profiles at each station. Water velocities from each ADCP deployment were rotated into an along- and across-shelf coordinate system defined by the principal axis of depth-averaged flow (Table 1). Time series of across-shelf surface transport were computed by extrapolating velocity profiles, assuming a constant velocity (slab) extrapolation, to the surface and bottom before subtracting the depth-averaged mean and integrating the profiles from the surface to the first zero crossing, following Kirincich et al. (2005). Pressure anomaly was calculated by subtracting a harmonic fit of the tidal variability, found using

TABLE 1. The 2004 PISCO mooring deployments. XTI and TBT are Onset XTI and Tidbit temperature loggers, SBE16 and SBE37 are Seabird CT loggers, and WH600 are RDI Workhorse 600-kHz ADCPs, with integrated pressure and temperature sensors. Velocity statistics are presented for the depth-averaged along and across-shelf velocities. The principal axis of flow (PA), in degrees east of true north, is listed for each deployment as is a local estimate of the quadratic drag coefficient (C_f; see appendix B).

	Station/deployment					
	LB	YB	LB	SR	YB	SH
	Early season		Late season			
Latitude (N)	44°51.500′	44°19.328′	44°51.500′	44°30.300′	44°19.328′	44°15.140′
Longitude (W)	124°03.374′	124°07.257′	124°03.374′	124°06.100′	124°07.257′	124°07.641′
Start day	133	135	192	191	190	191
End day	192	188	272	253	247	253
	Instrumentation					
Depth (m)						
1	TBT	XTI	TBT	XTI	XTI	TBT
4	TBT	XTI	TBT	XTI	XTI	TBT
8		SBE37		SBE37	SBE37	SBE16
9	TBT	XTI	TBT	XTI	XTI	TBT
11	SBE16		SBE16			SBE16
14	TBT	TBT	XTI	XTI	XTI	TBT
14.5	WH600	WH600	WH600	WH600	WH600	WH600
	Velocity statistics (m s^{-1})					
Alongshelf						
Mean	−0.068	−0.007	−0.034	0.023	−0.015	−0.041
Std dev	0.086	0.117	0.091	0.101	0.120	0.113
Across-shelf						
Mean	0.002	−0.003	−0.004	−0.000	0.001	0.005
Std dev	0.010	0.013	0.017	0.010	0.007	0.007
PA direction (deg)	24	8	23	1	10	7
Local C_f ($\times 10^3$)	1.9	0.7	3.4	2.3	1.3	1.6

T_TIDE (Pawlowicz et al. 2002), and the mean pressure (see appendix A) from the observed bottom pressure time series. Based on nearby CTD casts, temperature–salinity profiles have a linear relationship in the inner shelf during summer. The average slope of this relationship ($m = 8.4$°C psu^{-1}) was used, with the available salinity measurements, to estimate salinity and density at the location of each temperature measurement (Table 1).

Additional meteorological and tidal measurements collected at Newport, Oregon, by NOAA were used in the analysis. Winds at the Newport Coastal–Marine Automated Network (CMAN) station, located on the south jetty of the Newport harbor entrance, are considered representative of winds throughout the study area during summer (Kirincich et al. 2005). Hourly averaged wind velocities, having an accuracy of ± 1.0 m s^{-1}, were translated to 10-m height wind velocities using the assumption of a neutral atmosphere. Wind stress in the alongshelf direction was estimated using the empirical method given by Large and Pond (1981). A ''Newport'' pressure anomaly, composed of hourly averaged sea level height at the NOAA South Beach tidal station and atmospheric pressure at the CMAN station, was used for comparison with the pressure anomaly measured by the ADCPs.

As a result of instrument failures during the 2004 season, the analysis was split into two periods: early summer (before day 190) when velocity and pressure observations are available for stations LB and YB only and late summer (after day 190) when measurements are available from all stations. All time series shown were low-pass filtered using a filter with a 40-h half-power period to isolate the subtidal components. Additionally, all correlations given were tested for significance using a 95% confidence interval as noted in the text and table captions. The level of significance and confidence intervals were calculated using the effective degrees of freedom (N^*), calculated following Chelton (1983).

3. The 2004 upwelling season

During the summer of 2004, observed fluctuations of both alongshelf velocity and pressure anomaly at all stations were positively correlated with the observed, intermittently upwelling-favorable, wind stress. Early in the season, winds were to the south (negative) with northward (positive) reversals occurring almost weekly

(Fig. 2). A period of more persistent southward winds began after day 170 (18 June), as illustrated by a negative accumulation in the cumulative northward wind stress (Fig. 3). After this date, northward wind events occur approximately every 20 days, specifically near days 203, 220, and 238. In general, northward (southward) depth-averaged, alongshelf velocities occurred when winds were to the north (south) (Fig. 2). However, velocities lagged the wind by 3 to 19 h with lags generally increasing to the south (Table 2). Pressure anomalies, used here as a proxy for the across-shelf pressure gradient present during coastal upwelling or downwelling, were also positively correlated with the alongshelf wind stress throughout the season. Among the stations onshore of the bank (SR, YB, SH) and including Newport SSP (NP), pressure anomalies were well correlated (Table 2) and visually similar (Fig. 2) throughout the season. Correlations between pressure anomaly at LB and these other stations decreased in magnitude (Table 2) as the LB time series visually diverged from the others later in the season, most notably on days 203, 219–225, and 235–244 (Fig. 2).

Spatial variations in the mean alongshelf circulation (Table 1) can be illustrated by calculating the accumulated alongshelf velocities during each deployment. Early in the summer, station LB consistently accumulated negative (southward) alongshelf velocity throughout the deployment (Fig. 3). In contrast, station YB had a small negative velocity accumulation (Fig. 3) but larger magnitude fluctuations (Fig. 2, Table 1). After yearday 190 negative accumulation existed at station LB in the north as well as stations YB and SH in the south (Fig. 3). However, positive (northward) accumulation existed in the middle of the array at station SR. Velocity standard deviations at the three onbank stations were all larger than that found at LB (Table 1).

From these observations (Figs. 2 and 3), two flow regimes were apparent: a southward or near-zero alongshelf velocity present during upwelling favorable (southward) winds and a large northward velocity present during downwelling (northward) wind events. During upwelling winds, alongshelf velocities were 0.2 m s^{-1} to the south at station LB, near zero at station SR, 0.1 m s^{-1} to the south at station YB, and 0.2 m s^{-1} to the south at station SH (Fig. 2). Northward flow generally occurred at all stations during downwelling winds, with the largest velocities exceeding 0.3 m s^{-1} at station SR on yearday 238. The convergence of alongshelf velocities between stations LB and YB before day 190 and stations LB and SR afterward (Fig. 3) implies that southward flowing waters north of the bank are exported offshore throughout the summer. In addition, the velocity divergence between stations SR and YB after day 190 implies a mean onshore flow must exist between the two to conserve mass.

Time series of density (Fig. 2) were generally similar at all stations, as were time series of accumulated across-shelf transport (Fig. 3). A sharp increase in density occurred at the onset of strong upwelling on day 165, before which significant variability existed. During this persistent upwelling, density reached a maximum near 26 kg m^{-3} (thin lines in Fig. 2). The major wind reversals noted above corresponded with sharp decreases in density, reaching minimum values of 23.5–24.5 kg m^{-3} for 2–3 days. Early in the season, across-shelf transport accumulation (a psuedomeasure of across-shelf displacement) was negative (offshore) at both stations, with YB accumulating slightly larger values (Fig. 3). After days 190 to 203, when YB and SH only had positive (onshore) transport, all stations accumulate negative surface transport. Despite some station-to-station variations and onshore transport events, the total accumulated offshore transport for all four stations during the second half of the season was similar for LB, SR, and YB, but higher at SH.

4. Modes of variability

An empirical orthogonal function analysis was performed separately on time series of depth-averaged alongshelf velocity, pressure anomaly, midwater column density, and across-shelf surface transport from each of the four stations during the common time period of yeardays 190 to 250 (Fig. 2). These results, specifically the amplitude time series of the dominant EOF modes and the distribution of local variance explained by these modes, show the dominant patterns and spatial differences of circulation at the PISCO stations. To assess the local statistical significance of each mode, the level of significance was computed for each pair of raw and modal amplitude time series based on the correlation coefficient (the square root of the percent of local variance explained) and the effective degrees of freedom for the pair. Significant results (at the 95% confidence interval) for the first three modes for each EOF are shown in bold in Table 3. Owing to the unequal alongshelf station spacing, the spatial significance of the EOF results were tested by additional EOF analyses that either used only three equally spaced stations (SH, SR, and LB) or included data from an additional station (the Newport sea level height for the pressure anomaly EOF). All tests gave quantitatively similar results.

Of the significant results, two dominant modes of variability existed in each EOF. At the southern three stations, the mode-one results accounted for greater

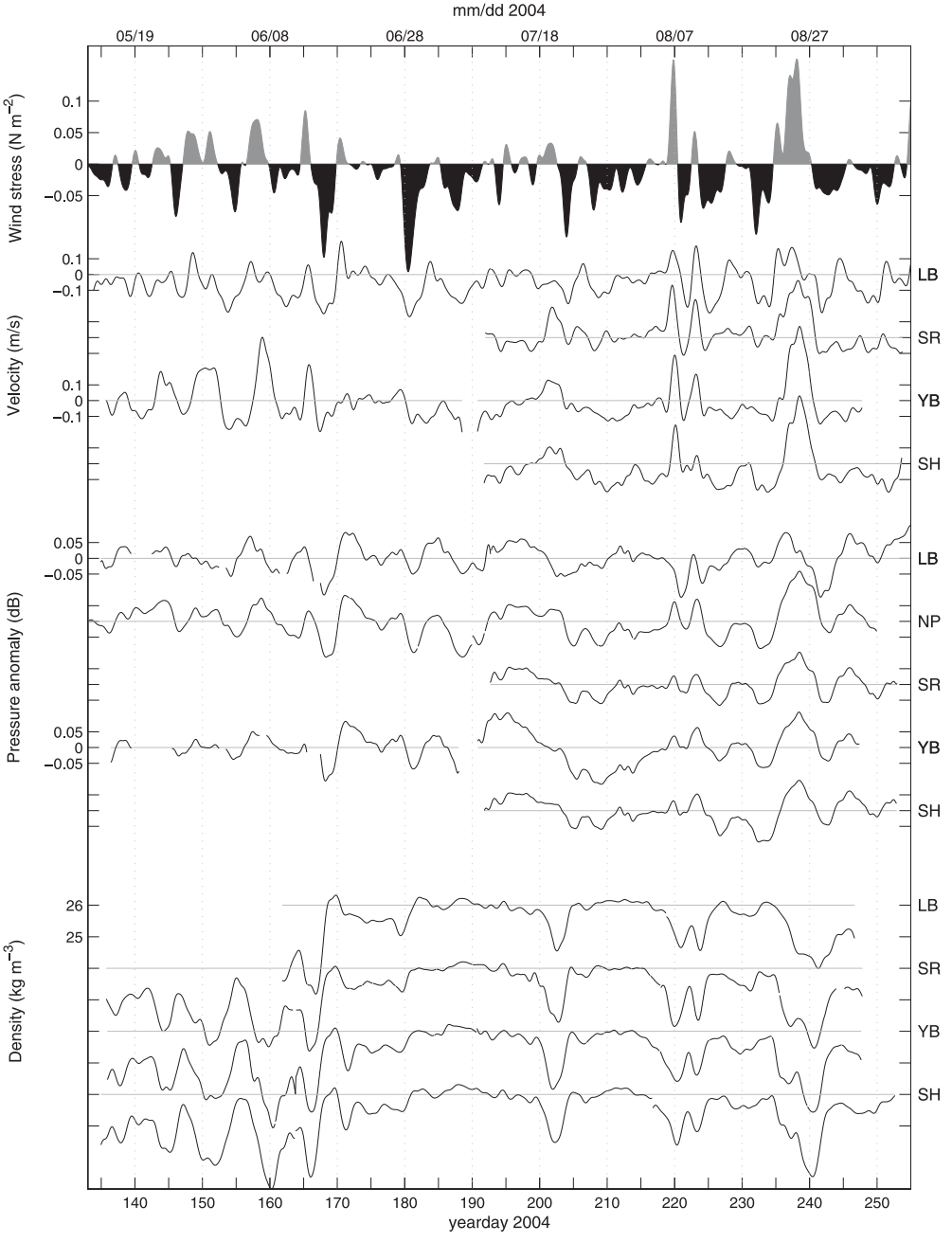

FIG. 2. Inner-shelf conditions during the 2004 upwelling season. North wind stress from the Newport CMAN station is shown above offset plots of depth-averaged, alongshelf velocity (m s^{-1}), pressure anomalies (db), and midwater density (kg m^{-3}) from each of the four stations. For each type, stations are plotted (top) north to (bottom) south. The Newport SSP (NP) is included among the pressure anomalies for reference. For each time series, thin lines mark the zero crossing (velocity and pressure) or 26 kg m^{-3} (density: 1000 kg m^{-3}). Tick increments for each are wind stress (0.05 N m^{-2}), water velocity (0.1 m s^{-1}), pressure (0.05 db), and density (1 kg m^{-3}).

than 86%, 69%, 68%, and 95% of the local variability for pressure, velocity, transport, and density (Table 3). However, at LB in the north, the local percent variances explained by this dominant mode were reduced, at 40%, 33%, 47%, and 82%, respectively. In many of the EOFs, a higher mode (mode two for pressure, velocity, but mode three for transport) accounted for the majority of the local variability at LB.

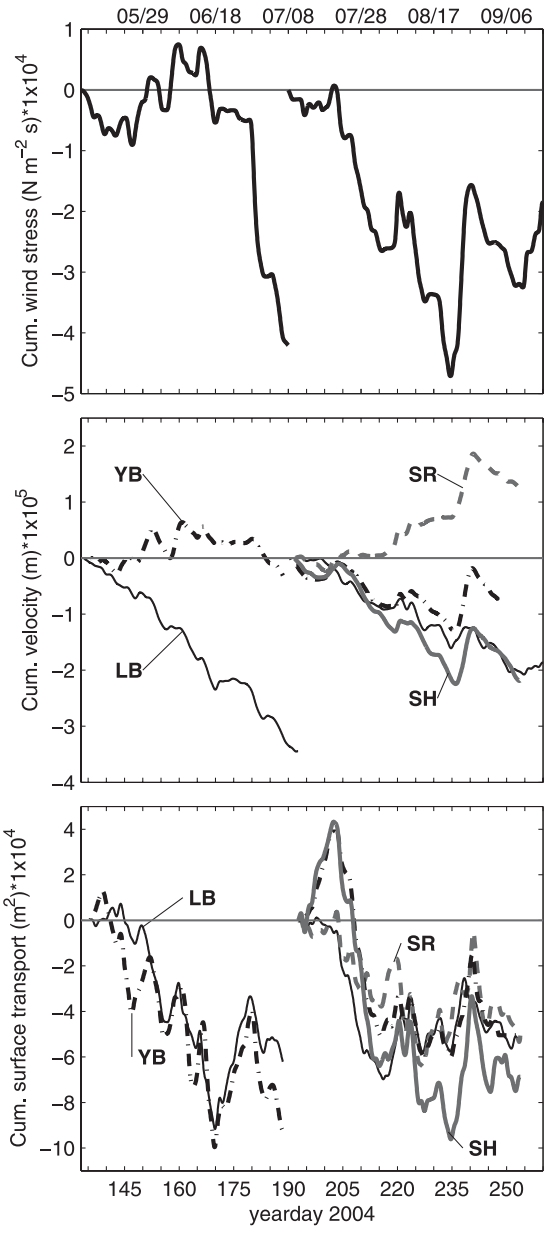

FIG. 3. (top) Cumulative alongshelf wind stress, (middle) cumulative depth-averaged alongshelf velocity, or alongshelf displacement, and (bottom) across-shelf surface transport between (left) days 133–190 and (right) days 190–273.

The dominant, mode-one pattern of variability from all four EOFs was characteristic of inner-shelf circulation driven by the local alongshelf wind forcing. Mode-one amplitude time series for pressure anomaly and alongshelf velocity (Fig. 4a) were positively correlated with the local alongshelf wind stress. A maximum correlation of 0.63 (0.87) occurred when pressure (velocity) lagged the wind by 6 (8) hours. Mode-one pressure and velocity were themselves significantly correlated at 0.60 (with pressure leading by 6 h). Also consistent with wind-driven upwelling circulation, the mode-one across-shelf surface transport (U_s) was well correlated (0.72 at 0 lag) with the theoretical Ekman transport ($U_{tek} = \tau_s^y/\rho f$) and, following Kirincich et al. (2005), had a regression coefficient between U_s and U_{tek} of $R = 0.19$. This mode-one fraction of full Ekman transport was slightly smaller than the mean of 25% found by Kirincich et al. (2005) for previous years, but within the range of variability reported. The potential effect of U_s on inner-shelf density was coherent between the mode-one EOF results. As shown in Fig. 4b, when U_s (or U_{tek} R) was positive (negative), the time rate of change of mode-one density ($\Delta\sigma_t/\Delta t$) was negative (positive) and inner-shelf density decreased (increased). The rapid variations of U_s near days 203, 220, and 235 were mirrored by larger values of $\Delta\sigma_t$; while during sustained upwelling (negative U_s; e.g., days 205–216), density changes were much smaller.

The remaining, second mode occurring only at station LB was part of a second distinct pattern of variability. This LB mode was uncorrelated with the local winds (not shown here). The LB-mode across-shelf transport (U_s) and alongshelf transport (V) were positively correlated (0.56 when velocity leads by 5 h). The LB-mode U_s and density time series were tightly coupled (Fig. 5b) in the same manner described for the wind-driven mode. These three time series can be related through a similar mechanism as described for mode one, but with forcing from the alongshelf velocity rather than the wind. A barotropic alongshelf velocity would result in across-shelf transport in a bottom Ekman layer and thus, using the coastal boundary condition, opposite across-shelf transport in the surface layer and isopycnal displacement. Yet, in a departure from the geostrophy found in mode one, LB-mode time series of pressure and velocity frequently appeared to be in quadrature (days 217–226 and 238–245 in Fig. 5). Investigating this pattern further, a phase and coherence diagram of mode-two pressure and velocity shows a peak at 0.3 cpd (2.18×10^{-5} s^{-1}) having a phase lag of 90° (Fig. 6). Using a 14-day moving cross-covariance between pressure and velocity (Fig. 6), this 0.3-cpd coherence peak appears due primarily to the larger oscillations of days 214–230, having significant lags at 20 h (and 100 h, the peak of the next cycle). During the remainder of the time series, LB-mode velocity and pressure are often most strongly correlated at near-zero lags. The possible source of the LB-mode fluctuations is discussed further in section 6.

5. Depth-averaged alongshelf momentum equation

An analysis of the depth-averaged, alongshelf momentum equation was performed using observations

TABLE 2. Early and late season depth-averaged, alongshelf velocity and pressure anomaly correlations (lags) with alongshelf wind stress. All correlations shown were statistically significant at the 95% confidence interval. Peak lagged correlations are substituted only when significantly different from the zero lag correlation. A negative lag (in hours) means the column time series (e.g., wind) leads the row time series (e.g., LB velocity).

	Early season (days 133–190)			Late season (days 190–255)				
Station	Wind	LB	YB	Wind	LB	SR	YB	SH
				Velocity				
LB	0.71 (−5)	1		0.73 (−4)	1			
SR				0.76 (−3)	0.55	1		
YB	0.65 (−19)	0.51 (−13)	1	0.79 (−9)	0.45	0.84	1	
SH				0.78 (−12)	0.53 (−39)	0.73	0.93	1
				Pressure				
LB	0.53 (−1)	1		0.42 (10)	1			
SR				0.71 (−8)	0.64 (−9)	1		
YB	0.68 (−7)	0.83 (−4)	1	0.53 (−12)	0.43 (−11)	0.84	1	
SH				0.60 (−9)	0.50 (−10)	0.91	0.79	1
NP	0.74 (13)	0.72 (−9)	0.94	0.75 (12)	0.45 (−20)	0.92	0.79	0.89

available from the PISCO array. Written with all terms on the left-hand side as

$$\frac{\partial \bar{v}}{\partial t} + f\bar{u} + \frac{1}{\rho_o}\frac{\partial \bar{p}}{\partial y} - \frac{\tau_s^y}{\rho_o h} + \frac{\tau_b^y}{\rho_o h} + \frac{\partial \overline{uv}}{\partial x} + \frac{\partial \overline{v^2}}{\partial y} = 0, \quad (1)$$

u and v are the across- and alongshelf depth-dependent velocity components (where the overbar denotes depth averaging), $\partial\bar{p}/\partial y$ is the alongshelf pressure gradient, $h = 15$ m, $\rho_o = 1025$ kg m^{-3}, $f = 1 \times 10^{-4}$ s^{-1}, τ_s^y and τ_b^y are the alongshelf wind and bottom stresses, and the two advective terms are written as momentum fluxes using mass conservation. Except for the wind stress, described in section 2, all terms were estimated at each station using the methods described in appendix B. Of the resulting time series, the Coriolis acceleration was at or below its measurement uncertainty (Table 4) and generally uncorrelated with other terms as u was minimized in the principal axis coordinate system used here. These small Coriolis values were consistent with the midshelf results of Allen and Smith (1981) for the Oregon shelf and the inner-shelf results of Lentz et al. (1999). The alongshelf flux of alongshelf momentum [the seventh term in (1)] was also small relative to other terms and generally not dynamically important. These two terms were not included further.

Time series of the remaining terms in (1) were used to assess the term interactions present during wind-forced upwelling, downwelling, and relaxation events on the Oregon inner shelf. The possible variations in inner-shelf dynamics occurring north of the bank versus onshore of the bank are evident in a comparison of these interactions at stations YB, an onbank station, and LB, the offbank station. Results for the onbank stations SR and SH were similar to those of YB. A two-point pressure gradient between LB and YB, with an uncertainty of 1.7×10^{-6} m^2 s^{-2} (see appendix B for methods), was used for the gradient at both stations during days 133–190 (Fig. 7). For days 190 to 248 (Fig. 8), an LB–SR pair is used at station LB while the SR–SH pair was used at station YB, both having larger uncertainties of 3.3×10^{-6} m^2 s^{-2}. It should be noted that use of the PISCO stations to calculate gradients arbitrarily sets the spatial scale of pressure fluctuations. Additional error, above the stated instrument uncertainties, may exist if the

TABLE 3. EOF results during days 190–250 for the first three modes for pressure anomaly, depth-averaged alongshelf velocity, across-shelf surface transport, and density. For the local percent variance explained by each EOF mode, statistically significant (at 95% confidence) percentages and modal amplitudes are listed in bold.

	Variance (%)					Amplitude			
Mode	Total	LB	SR	YB	SH	LB	SR	YB	SH
				Pressure anomaly (P dB)					
1	**77**	**40**	**94**	**86**	**89**	**−0.70**	**−0.93**	**−1.31**	**−0.98**
2	**17**	**59**	0	8	2	**1.80**	0.11	−0.82	−0.28
3	**6**	1	3	6	**14**	−0.38	0.55	−1.25	**1.41**
				Alongshelf velocity (m s^{-1})					
1	**79**	**33**	**69**	**95**	**84**	**−0.66**	**−1.01**	**−1.16**	**−1.10**
2	**14**	**60**	2	3	5	**1.75**	0.24	−0.41	−0.84
3	**6**	8	**28**	0	9	−0.70	**1.60**	−0.02	0.99
				Across-shelf surface transport (m^3 s^{-1})					
1	**73**	**47**	**68**	**78**	**86**	**−0.59**	**−1.06**	**−0.90**	**−1.30**
2	**14**	1	**31**	3	8	0.22	**−1.68**	0.42	0.97
3	**5**	**52**	0	1	2	**1.89**	−0.13	−0.25	−0.58
				Density (σ_t)					
1	**95**	**82**	**96**	**96**	**95**	**−0.87**	**−1.07**	**−1.04**	**−1.00**
2	**5**	**17**	0	3	2	**1.73**	−0.04	−0.75	−0.68
3	**1**	0	3	0	2	−0.45	1.51	0.01	1.23

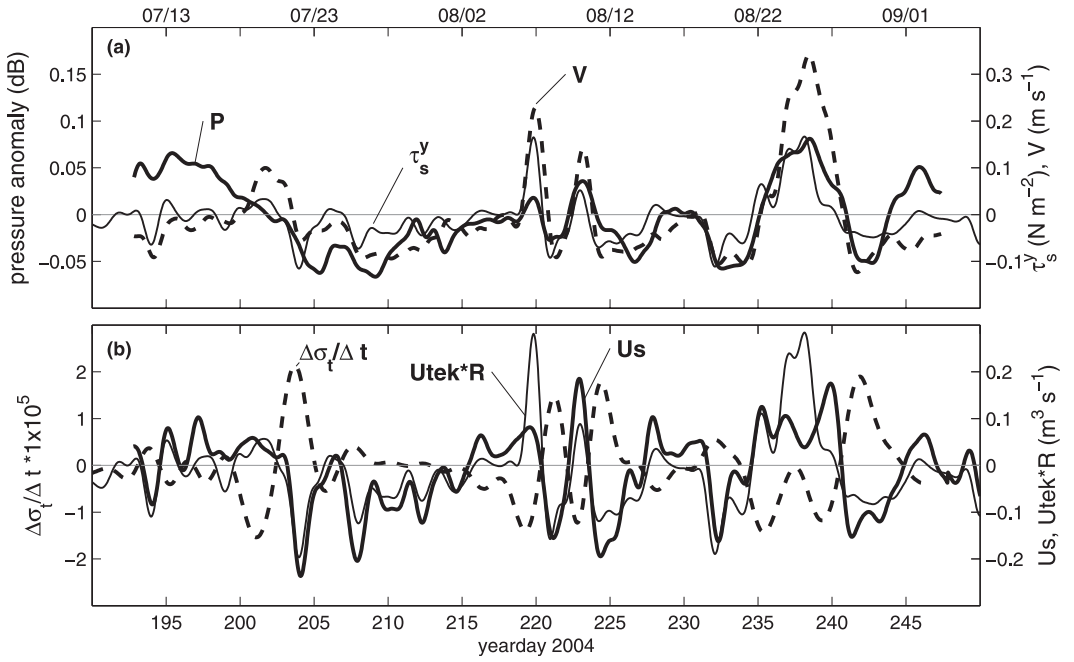

FIG. 4. Mode-one EOF amplitude time series for (a) pressure anomaly and depth-averaged alongshelf velocity and (b) across-shelf surface transport and the time rate of change of density anomaly. Alongshelf wind stress is included in (a) while the theoretical full Ekman transport (U_{rek}), multiplied by the neutral regression coefficient (R), is included in (b).

dynamically correct scale of pressure fluctuations differs from that set by the sensor locations.

Upwelling dynamics at LB and YB can be best understood by examining three upwelling wind events (days 145–147, 166–170, and 203–208.5: marked by solid lines in Figs. 7 and 8) in detail. In the first event (days 145–147), after the onset of an upwelling wind stress (a positive momentum source), a negative acceleration

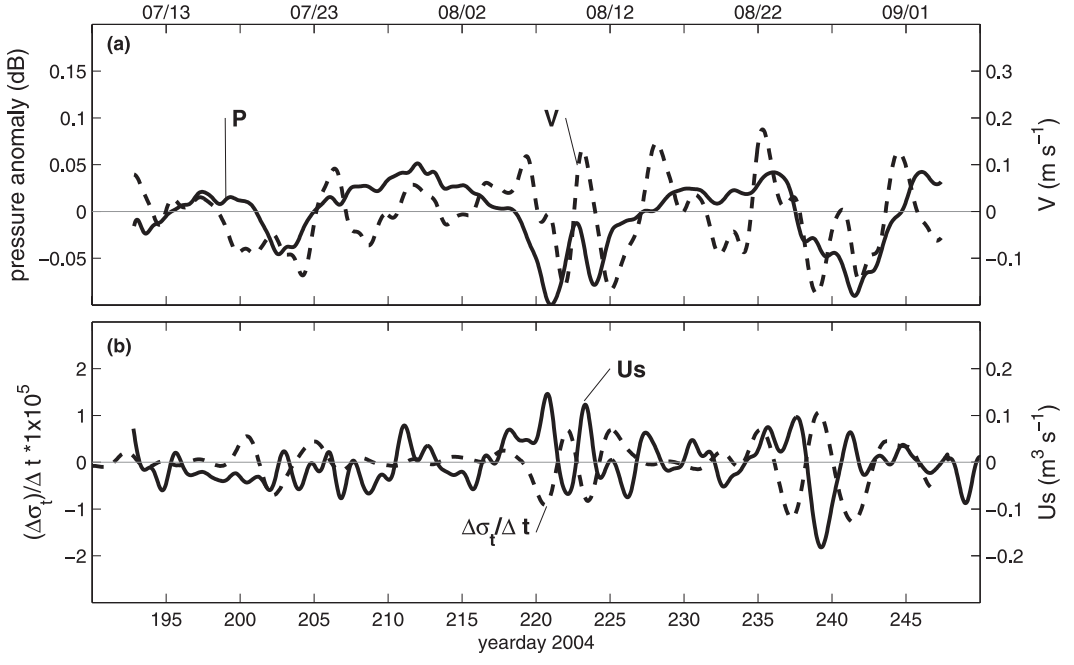

FIG. 5. Mode-two EOF amplitude time series for (a) pressure anomaly and depth-averaged alongshelf velocity and (b) across-shelf surface transport and the time rate of change of density anomaly.

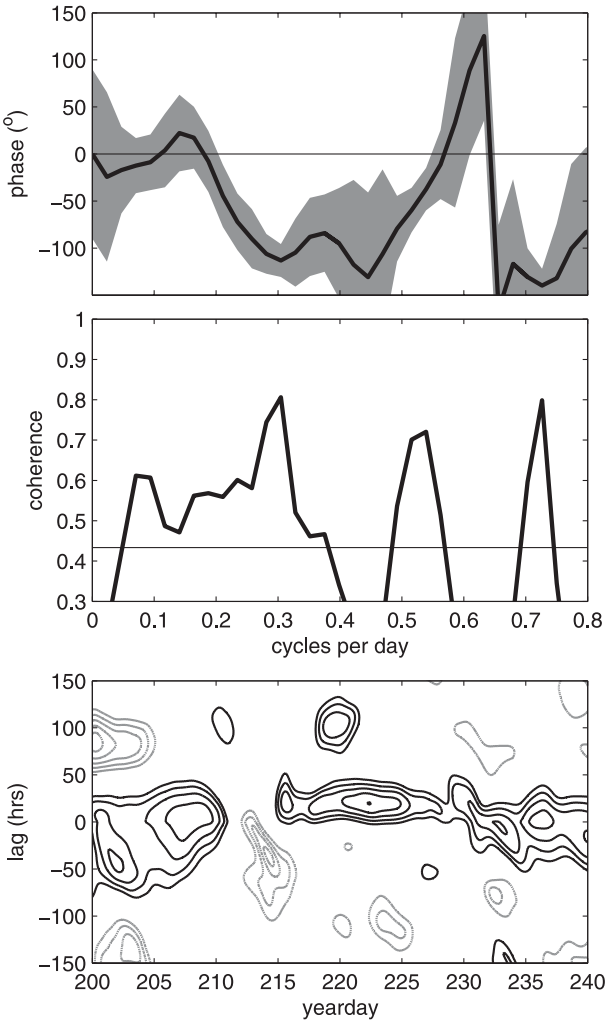

FIG. 6. (top) Phase and (middle) coherence of the mode-two EOF amplitude time series for depth-averaged alongshelf velocity vs pressure anomaly. The 95% confidence interval is shaded for phase and marked by the horizontal line for coherence interval. Positive phase differences indicate where pressure leads velocity. (bottom) A moving 2-week windowed cross-covariance between mode-two velocity and pressure. Correlation coefficients greater than +0.4 (solid) or less than −0.4 (dashed) are contoured in increments of 0.1. Positive lags indicate where pressure leads velocity.

initially increased in magnitude to balance the wind stress followed shortly by an increase in negative bottom stress (Figs. 7a,c). However, acceleration and bottom stress did not fully balance the wind, as would occur in the classic 2D upwelling balance (Allen and Smith 1981), and a nonzero residual of the three exists (2D-res: Figs. 7b,d). During this first event, the alongshelf pressure gradient, aided by the across-shelf momentum flux at YB, appears to offset 2D-res at both stations with an opposing structure. During the second event (days 166–170), the bottom stress response was weaker at station YB, resulting in a larger 2D-res compared to LB. The across-shelf momentum flux, small at LB, offset most of 2D-res at YB as the estimated alongshelf pressure gradient was incomplete owing to anchor shifts (see appendix A). Throughout the third event (days 203–208.5; Fig. 8), a series of two upwelling wind pulses, acceleration, and bottom stress generally combined to oppose the variable wind stress at LB while the resulting 2D-res was unrelated to the much larger pressure gradient. In contrast, due to a small bottom stress at YB, 2D-res was as large as 0.75×10^{-5} m s^{-2} during the upwelling peaks. Here, the negative across-shelf momentum flux and pressure gradient clearly offset the positive 2D-res (Fig. 8d).

TABLE 4. Uncertainty estimates for terms in the alongshelf momentum balance terms (m s^{-2})* 1×10^6 at each station. Terms are acceleration (acc), Coriolis (cor), wind stress (ws), bottom stress (bs), pressure gradient (pg), across-shelf momentum flux (xsmf), and alongshelf momentum flux (asmf).

	Station/deployment					
	LB	YB	LB	SR	YB	SH
Term	Early season		Late season			
acc	0.3	0.3	0.3	0.3	0.3	0.3
Cor	1	1	1	1	1	1
ws	0.9	0.9	0.9	0.9	0.9	0.9
bs	0.01	0.01	0.02	0.02	0.01	0.01
pg	1.6	1.6	3.3	3.3	3.3	3.3
xsmf	0.1	0.1	0.1	0.1	0.1	0.1
asmf	0.01	0.01	0.01	0.01	0.01	0.01

Variable term interactions were also found during downwelling wind events. During the strong downwelling events (days 219–220 and 236–240; the shaded areas of Fig. 8), both acceleration and bottom stress increased rapidly to balance the negative momentum of the wind stress at YB. This reaction of acceleration and bottom stress was not as strong at station LB, resulting in a large, unbalanced 2D-res during both events.

Two sizable relaxation events (days 176.5–178.5 and 216–219, marked by dashed lines in Figs. 7 and 8) occurred during the study period. In the first event (days 176.5–178.5), with an initial balance between 2D-res (dominated by the wind stress) and pressure gradient at YB (Figs. 7c,d), the decreasing wind stress was replaced by acceleration as the pressure gradient remained constant and bottom stress remained small. At LB the same decreasing wind was initially offset by acceleration until bottom stress changed sign and acceleration became negative (Figs. 7a,b). During the second event (days 216–218), as winds decreased on day 216, 2D-res at YB was initially balanced by the across-shelf momentum flux. On day 217 acceleration became increasingly positive as the pressure gradient became increasingly negative.

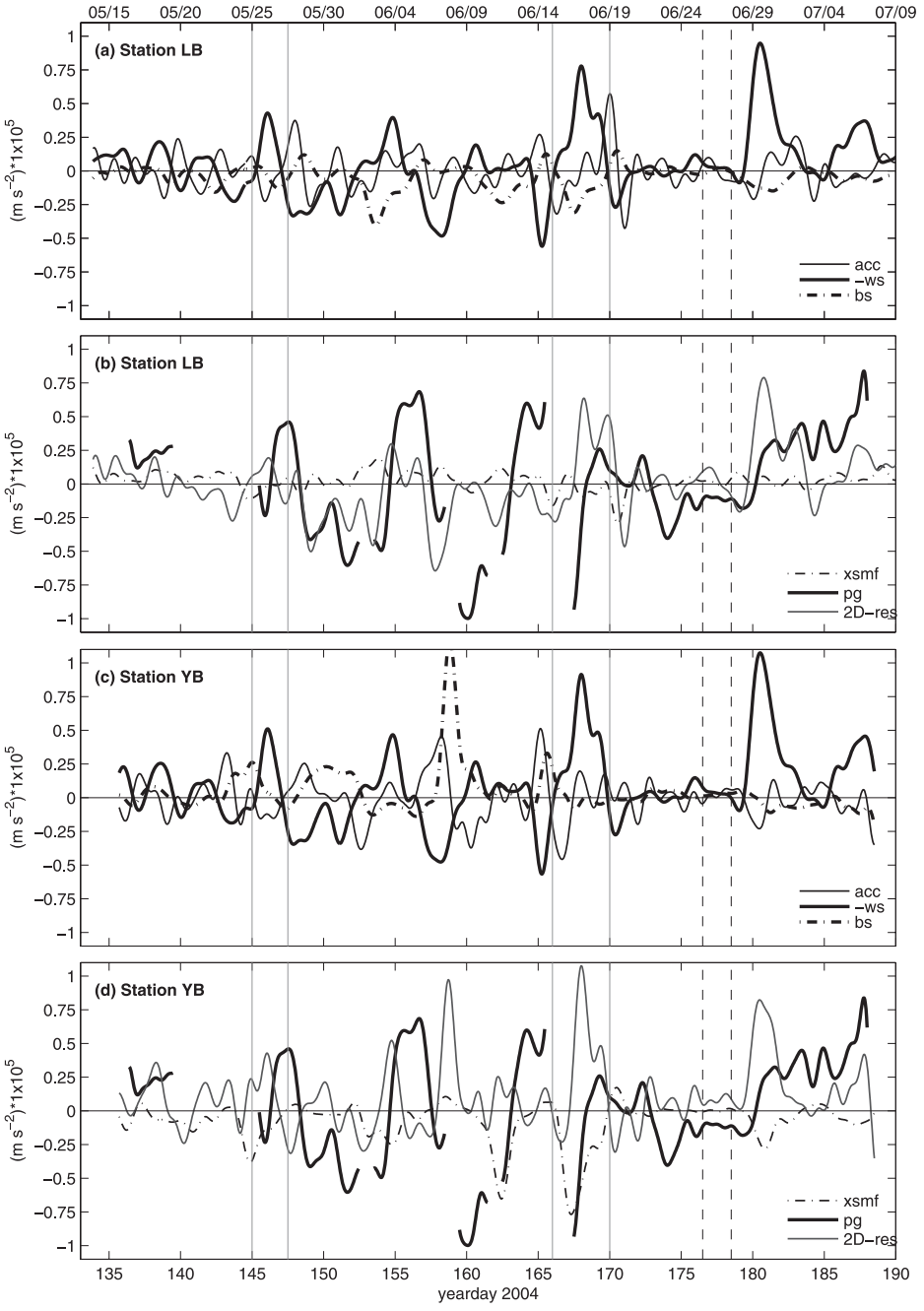

FIG. 7. Terms in the depth-averaged, alongshelf momentum balance at (a),(b) the offbank station, LB, and (c),(d) onbank station, YB, for days 133–190. Legend labels are acceleration (acc), wind stress (ws), bottom stress (bs), across-shelf momentum flux (xsmf), pressure gradient (pg), sum of the acceleration and stresses (2D-res). Pairs of vertical lines mark specific events described in the text.

Bottom stress then increased to balance the pressure gradient before interactions became unclear on day 218 with a larger negative acceleration term. At LB acceleration and bottom stress balance the decreasing wind at the beginning of this period before all terms, except for the unbalanced pressure gradient, become small.

The term interactions and alongshelf variations highlighted above for individual events are consistent with time-series-average interactions found by bin-averaging

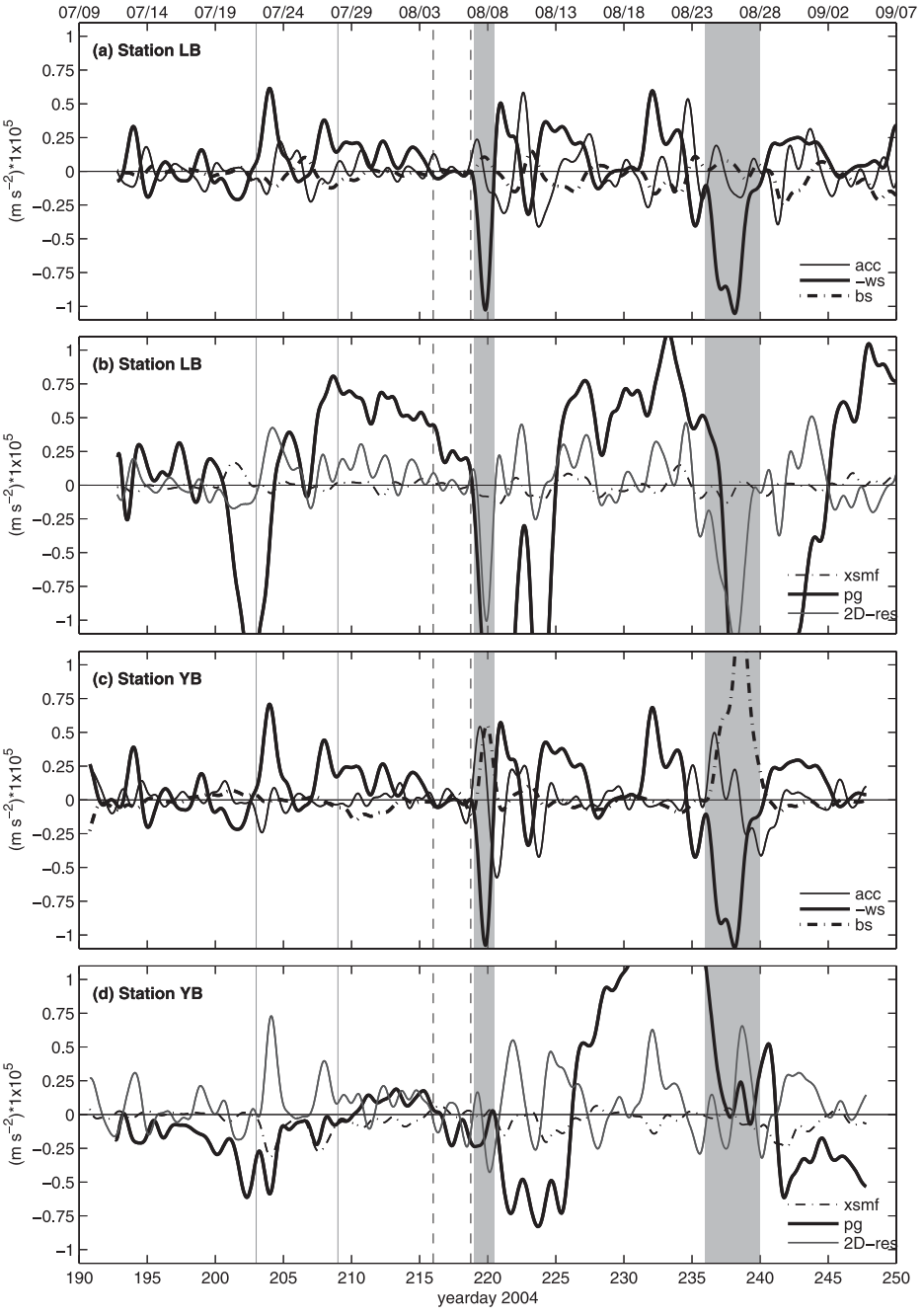

FIG. 8. Terms in the depth-averaged, alongshelf momentum balance at (a),(b) the offbank station, LB, and (c),(d) onbank station, YB, for days 190–250. Legend labels follow Fig. 7. Pairs of vertical lines, or shaded areas, mark specific events described in the text.

terms in the dominant balances described. Throughout both halves of the season, bottom stress at LB balanced more of the wind stress plus acceleration (−ws + acc) when this sum was positive (Fig. 9), generally occurring during upwelling favorable winds. In contrast, bottom stress at YB was stronger than at LB during downwelling favorable winds (negative −ws + acc), fully balancing the sum during peak events (Fig. 9). Acceleration was important to the depth-averaged alongshelf momentum balances at both stations. The sum of acceleration and the wind stress had increased magnitudes and correlations to bottom stress than wind stress alone.

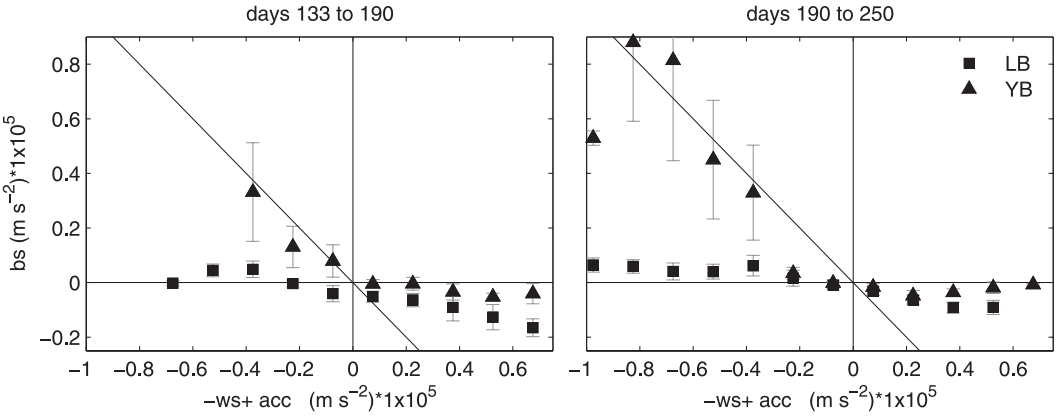

FIG. 9. Bin averages of bottom stress (bs) verses the sum of the wind stress and acceleration (−ws + acc) at stations LB and YB for (left) early season (days 133–190) and (right) late season (days 190–250). Standard error bounds, found using the effective degrees of freedom, are given for each bin. The one-to-one correspondence line, meaning that the average magnitude of bottom stress fully offsets the magnitude of the wind stress and acceleration, is shown on each panel.

Comparing the sum of these three terms (2D-res) to the across-shelf momentum flux (xsmf) in Fig. 10, the across-shelf flux of momentum was small at LB during all times yet consistently offset a portion of 2D-res at station YB when 2D-res was positive, generally occurring during upwelling favorable winds. This was especially true during the first half of the season. The alongshelf pressure gradient (pg) at YB consistently offsets most of 2D-res during the second half of the season, when the large and unbalanced gradient occurring from days 227 to 237 (Fig. 8d) was excluded. When 2D-res was small or negative, generally occurring during downwelling favorable winds, the YB pressure gradient offsets 2D-res during the first half of the season. However, for moderate, positive values of 2D-res at YB early in the season, the gradient was also positive. The bin-averaged pressure gradient during first half of the season at LB (not shown) was similar to that shown for YB (Fig. 10).

Despite the occurrences of balanced pressure gradients at LB during early season upwelling (e.g., day 145–147), relaxation (days 176.5–178.5), and weak winds events (days 198–201), the pressure gradient at LB became large and unbalanced after day 201 (Fig. 8b). These periods of large unbalanced gradients, well outside of the estimated instrument uncertainty for this term (Table 4), were somewhat expected given the second mode of pressure variability occurring only at LB. The

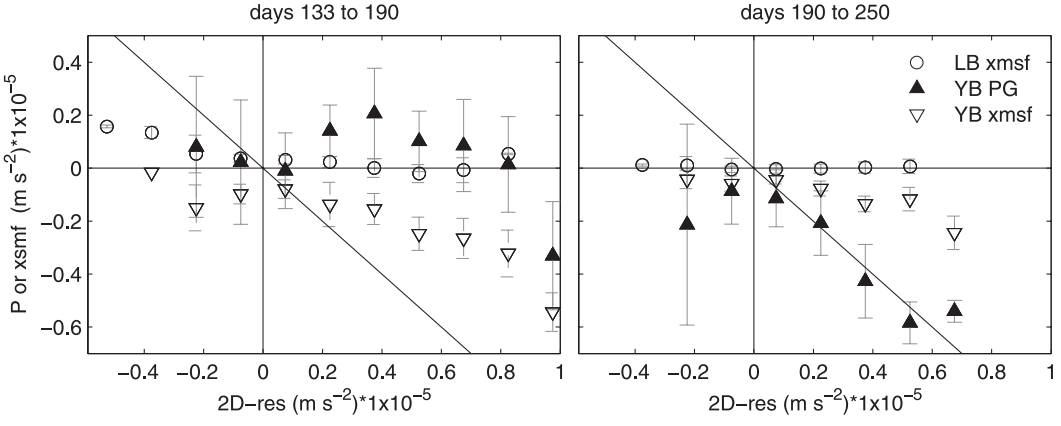

FIG. 10. Bin averages of the pressure gradient (pg) or across-shelf momentum flux (xsmf) vs 2D-res at stations LB and YB for (left) early season (days 133–190) and (right) late season (days 190–250). Bin-averaged pg at station LB is not shown, as it was similar to YB pg for days 133–190 and unrepresentative of the true gradient at LB after day 201 (see text). Standard error bounds, found using the effective degrees of freedom, are given for each bin. The one-to-one correspondence line, meaning that the average magnitude of pg or xsmf fully offsets the magnitude of 2D-res, is shown on each panel.

measured gradient between LB and SR was similar to the mode-two pressure time series at LB (as is evident from the strong correspondence of pressure fluctuations in Figs. 5 and 8b) after day 201, indicating that the mode-two fluctuations at LB dominated the pressure difference between the stations. During these times, this observed gradient was unlikely to be representative of the true gradient at station LB. Mode-two variability did not occur inshore of the bank, thus the dynamically important along-stream variations of mode-two pressure were not measured by pressure array. The bin-averaged pressure gradient at LB for the second half of the season was not shown in Fig. 10 for this reason.

6. Discussion

This description of inner-shelf circulation along the central Oregon coast agrees well with the known middle- and outer-shelf circulation described earlier, which together can be summarized using the cartoon found in Fig. 11. The convergent flow between LB and SR, inferred from spatial variations of cumulative alongshelf velocities (Fig. 3), was consistent with observations of offshore transport of the main upwelling jet between LB and SR in recent hydrographic surveys (Castelao and Barth 2005; Barth et al. 2005b). In addition, a northeastward flow onto the northern part of the bank from the southwest was also found in these surveys, consistent with the inferred divergence between SR and YB. The alongshelf spinup of a smaller scale upwelling circulation (a mini-jet) onshore of the bank, inferred here from the strengthening southward velocities between SR and SH, has been shown by previous shelfwide observations (Barth et al. 2005b; Kosro 2005) and numerical models (Oke et al. 2002; Gan and Allen 2005). The link between the dominant EOF mode and local wind forcing has been noted in EOF analyses of the middle and outer shelf (Kosro 2005; Oke et al. 2002) and spatial amplitudes of the mode-one pressure EOF match the onbank/offbank variations observed by Barth et al. (2005a,b) using dynamic height analysis. The variability not accounted for by this mode at SR, YB, and SH is likely related to the alongshelf spin up of the mini-jet. From these favorable comparisons, it is clear that the 2004 season was typical of conditions in the region and that the results described here fill the inner-shelf gap in our knowledge of the regional circulation.

In contrast to the onbank stations, station LB was forced both by these local winds as well as a second mode of variability. One explanation for this LB mode might be that it, combined with the first mode, shows a delayed or complex movement of the regional upwelling jet, which only station LB was exposed to, in response to the integrated wind forcing (see discussion by Austin and Barth 2002). A similar second mode of variability exists offshore of LB in the surface current EOF results of Kosro (2005), similarly modifying the wind-forced first mode. The regional model results of Oke et al. (2002) also appear to show a two mode system in the area, but ascribe the second mode to relaxation events only. It is tempting to infer that the 0.3-cpd coherence peak between mode-two pressure and velocity is the signature of remotely forced coastal-trapped waves (CTWs). This peak is similar to one reported by Huyer et al. (1975), based on late summer (July to September) observations of sea level at Depoe Bay (5.5 km south of LB) and alongshelf velocities at station NH-10 (offshore of Newport in 80 m of water), which could not be attributed to the local wind forcing. The phase relationship found here (quadrature) is not characteristic of free, unforced CTWs, and phase information for this peak in Huyer et al. (1975) was not significant. Yet, the coastal-trapped wave results of Chapman (1987) do show a similar phase lag between pressure and velocity in the Coastal Ocean Dynamics Experiment (CODE) region (his Figs. 9 and 10). Additional upwelling season observations in the region (Cutchin and Smith 1973; Allen and Smith 1981; Kundu et al. 1975; Battisti and Hickey 1984) using the Newport sea level station did not observe the 0.3-cpd

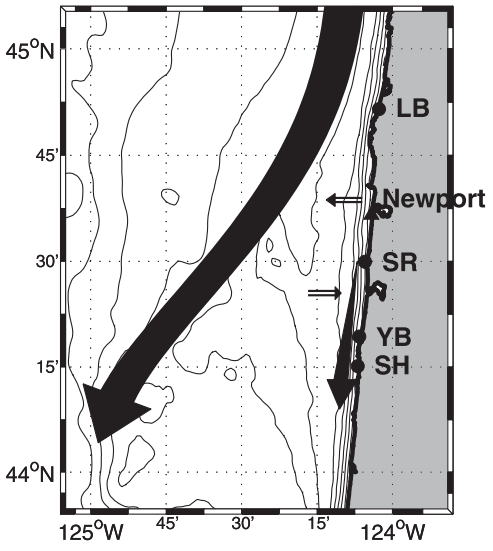

FIG. 11. Cartoon of regional upwelling circulation on the central Oregon shelf during late summer: The core of the coastal jet (large solid arrow) is diverted offshore and around the Heceta and Stonewall Bank complex by flow–topography interactions that cause offshore, cross-isobath transport north of station SR (small open arrow). In the lee of this circulation a smaller upwelling jet (small solid arrow) spins up in the inner-shelf south of Newport. The region offshore of this secondary jet, and over the bank, is characterized by weak, onshore velocities (small open arrow).

coherence structure reported here and in Huyer et al. (1975). Our results show that, during late summer, the Newport sea level was closely related to pressure at the onbank stations (Table 2), all of which were presumably sheltered from this second mode by the bank. Despite these differences, the total across-shelf transport at LB, was similar in magnitude to that found at the onbank stations (Fig. 3).

These spatial variations in inner-shelf circulation appeared to develop over the course of the summer as the regional upwelling circulation intensified. Based on the accumulated alongshelf velocities (Fig. 3), weak southward alongshelf flow existed at YB early in the season but shifted north to SR as the secondary upwelling circulation intensified at YB later in the season. In the alongshelf momentum equation, magnitudes of across-shelf momentum flux relative to 2D-res decreased over time at both stations. At LB this term was small for negative 2D-res before day 190, but near zero for all 2D-res after day 190 (Fig. 10). At YB across-shelf momentum flux offsets most of 2D-res before day 190, while the pressure gradient does so after day 190. The occurrence of balanced, then unbalanced, pressure gradients throughout the season, particularly at station LB, implies that the alongshelf scale of the gradient varied over the season. Early in the season the gradient appears to be long, as it was often resolved by sensors 60 km apart during the upwelling and relaxation events highlighted here. Later in the season, however, the onbank gradient was well resolved by sensors 27 km apart (at SR and SH), but the array was unable to resolve the dynamically important gradient at LB, 30 km north of SR.

Of the results shown for the depth-averaged, alongshelf momentum equation, the importance of acceleration and across-shelf momentum flux were particularly noteworthy. At all stations, acceleration played an important part in the momentum balance. Dynamically, acceleration balanced a changing wind stress as the change propagated through the water column, allowing an opposing bottom stress to develop. Additionally, a positive acceleration balanced the negative pressure gradient throughout relaxation events, or until the positive bottom stress associated with northward flow developed. The importance of alongshelf acceleration in deeper waters along the Oregon coast was noted by Allen and Smith (1981) for time scales less than 10 days. Model studies (Gan and Allen 2002; Oke et al. 2002) have reported similar balances between acceleration and the pressure gradient during relaxation events, although not in the area of station LB (Oke et al. 2002). Closer to shore, the importance of acceleration has been noted by others (Lentz et al. 1999; Liu and Weisberg 2005), yet not usually at water depths as shallow as 15 m. The stronger accelerations found at these stations might be due to the stronger stratification found, compared to previous inner-shelf studies. With mean buoyancy frequencies (N) of 0.013 s^{-1}, this level of stratification might make the water column appear more inviscid, slowing the transfer of stress through the water column. Yet, while stratification varied considerably over the season (N = 0.008 to 0.02 s^{-1}), the magnitude of the acceleration term was more closely linked to changes in the wind stress than changes in stratification. Thus, it appears that stronger stratification, combined with the intermittent wind forcing present, may have enabled the larger accelerations seen.

Perhaps the largest spatial difference in the alongshelf momentum balance was the large magnitude of across-shelf momentum flux at the onbank stations. This term, with the pressure gradient, frequently balanced the wind stress during upwelling at YB where bottom stress was small. The role of across-shelf momentum flux in balancing the wind during upwelling was illustrated by Lentz and Chapman (2004) for outer-shelf observations but, to our knowledge, has not been observed in the inner shelf. The importance of this term at these shallow depths along the Oregon coast contrasts with the model results of Oke et al. (2002), who found that bottom stress and acceleration primarily balanced the wind inshore of the 50-m isobath. A predictive theory for the importance of the across-shelf momentum flux was given by Lentz and Chapman (2004), who found that the magnitude of the momentum flux relative to the wind stress depended on the Burger number, $S = \alpha N/f$. Using the observed stratification at YB to estimate the buoyancy frequency, and a bottom slope of α = 0.0125 (Kirincich et al. 2005), we estimate a Burger number of S = 1.2 to 2.1. This range (due to variable stratification) is characteristic of the strong stratification regime where bottom stress is reduced and the momentum flux is predicted to primarily balance the wind stress during upwelling. In contrast, with similar levels of stratification, and thus similar Burger numbers, a stronger bottom stress opposed the wind at LB (Fig. 9), as vertical shear was reduced (not shown here). During this time, the across-shelf momentum flux was small at LB (Fig. 9). The cause for the breakdown of Lentz and Chapman's (2004) theory at LB is not known. Lacking a viable alongshelf pressure gradient during many of the upwelling events as well as additional stations with the same two mode structure, we are unable to determine what balances the remainder of the wind forcing at LB, or if local three-dimensional effects play a role in the observed circulation.

Finally, previous studies (Leslie et al. 2005; Barth et al. 2005a) have suggested a link between the low flow area over the bank offshore and increased primary

production and consumers onshore. The alongshelf differences in inner-shelf circulation found here make this connection stronger, explaining a number of known alongshelf variations in the growth and reproduction of nearshore invertebrate species. From the divergence of cumulative alongshelf transport between SR and SH, we infer that onshore flow from the bank (known to be high in chlorophyll *a*) may feed the southward flowing minijet. Perhaps as a result, Leslie et al. (2005) found that intertidal chlorophyll *a* concentrations were consistently higher onshore of the bank at SH compared to LB north of the bank. This elevated chlorophyll was thought to lead to higher growth rates of both barnacles (*Balanus glandula*) and mussels (*Mytilus californianus*), and higher larval production of barnacles in these intertidal zones at the onbank stations (Leslie et al. 2005). In addition, the seasonal development of this circulation pattern appears to explain the location and timing of mussel larval recruitment. The stagnation point of alongshelf flow on the inner shelf shifted northward from station YB early in the season to station SR later in the season as the mini-jet jet circulation spun up over time. Although recruitment is generally elevated between May and August in the region (Connolly et al. 2001), recruitment of mussels at stations YB and SR are higher than at all other sites to the north and south (Barth et al. 2007). Peak recruitment at these stations, occurring in July at YB and September at SR (Barth et al. 2007), moves northward as the season progresses over roughly the same time scale as the stagnation point of inner-shelf alongshelf flow moves from YB to SR.

7. Conclusions

This study has investigated the inner-shelf circulation along the central Oregon coast during the summer upwelling season. Within a 70-km-long region centered at Newport, Oregon, circulation at three alongshelf stations located onshore of a submarine bank differed from that of a station located north of the bank. During upwelling-favorable winds, strong southward alongshelf flow occurred north of the bank, no alongshelf flow occurred onshore of the northern part of the bank, and increasing southward flow occurred onshore of the southern part of the bank. During downwelling-favorable winds, inner-shelf waters onshore of the bank surged northward at magnitudes much larger then that found north of the bank. The alongshelf differences in inner-shelf circulation highlighted here appear to result from the effects of the submarine bank offshore on the regional upwelling circulation. Southward flowing waters from the northernmost station, LB, were diverted offshore along with the regional upwelling circulation. Isolated from the regional circulation, a smaller upwelling circulation spins up on the inner shelf inshore of the bank. As a result, circulation onshore from this bank was driven primarily by local wind forcing, while flow north of the bank was only partially driven by local winds. A secondary mode of variability, related to the movement of the regional upwelling jet due to remote forcings, contributes the bulk of the variability evident north of the bank. With the time-dependent wind forcing present, acceleration was found to be an important term in the depth-averaged alongshelf momentum equation at all stations. Yet, dynamically different momentum balances existed among the stations. During upwelling, bottom stress and acceleration primarily balance the wind at LB, while bottom stress was weaker at the southern three stations where the across-shelf momentum flux and pressure gradient balanced the residual of the acceleration and stresses. During downwelling, wind stress and acceleration are fully balanced by bottom stress onshore of the bank. In contrast, additional unresolved sources of momentum are needed (e.g., the true pressure gradient) to balance downwelling favorable winds at LB. These alongshelf differences in inner-shelf circulation developed over the course of the summer as the regional upwelling circulation intensified; including the location of the minima of southward flow during upwelling and the length scale of the alongshelf pressure gradient. The circulation patterns described here begin to explain known variations in growth and recruitment of nearshore invertebrate species and, thus, have significant implications for the larval supply and connectivity in the region.

Acknowledgments. This is contribution 317 from PISCO, the Partnership for Interdisciplinary Studies of Coastal Oceans funded primarily by the Gordon and Betty Moore Foundation and David and Lucile Packard Foundation. We thank J. Lubchenco and B. Menge for establishing and maintaining the PISCO observational program at OSU as well as Captain P. York, C. Holmes, and S. Holmes for their data collection efforts. Additional support for JAB was provided by National Science Foundation Grant OCE-9907854.

APPENDIX A

Calculating the Pressure Anomaly

The pressure anomaly at each station was calculated from the measured bottom pressure by removing a pressure time series accounting for the mean and linear trend of pressure over the deployment period as well as sudden changes in pressure due to episodic movements

of the bottom lander. The PISCO sensors were particularly susceptible to these sudden shifts as the landers settled during the initial 40 days of the season (days 130–170). Thus, to maximize the length of the pressure records used in the analysis, a technique was developed to identify and eliminate pressure shifts using the ADCP's heading, pitch, and roll observations. The technique uses two assumptions: 1) Pressure shifts caused by lander movement are associated with changes in the instrument orientation and 2) the lander should only move down relative to sea level, thus mean pressure must increase over time. Following the first assumption, all potential shifts in a record were found using a metric of total daily orientation change, formed by the sum of hourly heading, pitch, and roll changes integrated over each day. All days with changes above a threshold of 2.3° per day (set by inspection) were flagged as potential shifts. Following the second assumption, a mean pressure was calculated for each individual ''unflagged'' period. If mean pressure increased between subsequent unflagged periods, a pressure shift occurred during the intervening flagged period and the flagged data was removed (causing the gaps occurring in the pressure records presented in Figs. 2 and 7). If the mean pressure decreased between subsequent unflagged periods, a pressure shift did not occur, the flag itself was removed, and the unflagged mean pressure was recalculated. Thus a time series of ''mean'' pressure from the remaining unflagged sections was subtracted from the measured bottom pressure, along with a linear trend and a tidal fit, to yield pressure anomaly. Potential errors might exist in the zero crossings of both pressure anomalies and pressure gradients as the mean pressure for each period was defined over different time scales for different stations.

APPENDIX B

Estimating Terms in the Alongshelf Momentum Balance

In Eq. (1) the acceleration and bottom stress terms were calculated directly from velocity observations at each station. Acceleration was calculated using three-point, centered finite differences of the alongshelf velocity ($\bar{v}$), while the Coriolis acceleration was calculated using ($\bar{u}$). Bottom stress was estimated with a quadratic parameterization, using velocities from the bottom ADCP bin (centered at 2.7 m above the bottom) and a drag coefficient of $C_f = 1.5 \times 10^{-3}$ (Perlin et al. 2005).

The depth-averaged, alongshelf pressure gradient can be written as the sum of the bottom pressure gradient and depth-averaged gradients of density throughout the water column:

$$\frac{\partial \bar{p}}{\partial y} = \frac{\partial p^b}{\partial y} - \frac{\partial}{\partial y}\left(\int_{-h}^{0} \rho g dz\right) + \frac{\partial}{\partial y}\left(\frac{1}{h}\int_{-h}^{0}\int_{z}^{0} \rho g dz dz\right), \tag{B1}$$

where $p^b(y)$ is the measured bottom pressure anomaly and $\rho(y, z)$ is the local density. The first two terms on the rhs comprise the sea level (or barotropic) pressure gradient, while the third term describes the depth-averaged water column (or baroclinic) pressure gradient. Estimates of the second and third terms of (B1), made from the time series of density profiles at each station, were an order of magnitude less than the first term derived from bottom pressure. Owing to the small magnitudes of these two terms and gaps in the density records, pressure gradients were calculated from the available station pairs (see text) using the bottom pressure term only.

The two nonlinear advective terms in Eq. (1) were estimated from products of unfiltered hourly velocities, depth-averaged, and then low-pass filtered. The across-shelf advection of alongshelf momentum ($\partial \overline{uv}/\partial x$) was estimated using the gradient of the velocity product between the mooring (1 km offshore) and the coast where the velocity product must be zero, following Lentz and Chapman (2004). The alongshelf advection of alongshelf momentum ($\partial \overline{v^2}/\partial y$) was estimated using differences between the same station pairs used to estimate pressure gradients.

Uncertainties of each term in the momentum balance, given in Table 4, were estimated based on the measurement accuracies and calculated as were the terms themselves, following methods used by Lentz et al. (1999). Uncertainty of the subtidal acceleration was based on the velocity error and a 10-h time period. Bottom stress uncertainty depends greatly on the appropriateness of the frictional coefficients used. A second estimate of C_f was obtained by minimizing the variance of the sum of the acceleration, wind stress, and bottom stress terms for each deployment, assuming they compose the dominant mean balance. The mean of these estimates, ranging from 0.7 to 3.4 ($\times 10^{-3}$) (Table 1) was similar to the $C_f = 1.5 \times 10^{-3}$ reported by (Perlin et al. 2005) and used here. Pressure gradient uncertainties were calculated as $(1/\rho)\Delta P/\Delta y$ where $\Delta P = 1$ mbar, the rms difference from the paired casts.

REFERENCES

Allen, J. S., and R. L. Smith, 1981: On the dynamics of wind-driven shelf currents. *Philos. Trans. Roy. Soc. London,* **A302,** 617–634.

Austin, J. A., and J. A. Barth, 2002: Variation in the position of the upwelling front on the Oregon shelf. *J. Geophys. Res.,* **107,** 3180, doi:10.1029/2001JC000858.

——, and S. J. Lentz, 2002: The inner shelf response to wind-driven upwelling and downwelling. *J. Phys. Oceanogr.,* **32,** 2171–2193.

Barth, J. A., S. D. Pierce, and R. M. Castelao, 2005a: Time-dependent, wind-driven flow over a shallow midshelf submarine bank. *J. Geophys. Res.,* **110,** C10S05, doi:10.1029/2004JC002761.

——, ——, and T. J. Cowles, 2005b: Mesoscale structure and its seasonal evolution in the northern California Current System. *Deep-Sea Res. II,* **52,** 5–28.

——, and Coauthors, 2007: Delayed upwelling alters nearshore coastal ocean ecosystems in the northern California Current. *Proc. Natl. Acad. Sci. USA,* **104,** 3719–3724.

Battisti, D. S., and B. M. Hickey, 1984: Application of remote wind-forced coastal trapped wave theory to the Oregon and Washington coasts. *J. Phys. Oceanogr.,* **14,** 887–903.

Castelao, R. M., and J. A. Barth, 2005: Coastal ocean response to summer upwelling favorable winds in a region of alongshore bottom topography variations off Oregon. *J. Geophys. Res.,* **110,** C10S04, doi:10.1029/2004JC002409.

Chapman, D. C., 1987: Application of wind-forced, long, coastal-trapped wave theory along the California coast. *J. Geophys. Res.,* **92** (C2), 1798–1816.

Chelton, D. B., 1983: Effects of sampling errors in statistical estimation. *Deep-Sea Res.,* **30,** 1083–1101.

Codiga, D. L., 2005: Interplay of wind forcing and buoyant discharge off Montauk Point: Seasonal changes to velocity structure and a coastal front. *J. Phys. Oceanogr.,* **35,** 1068–1085.

Connolly, S. R., B. A. Menge, and J. Roughgarden, 2001: A latitudinal gradient in recruitment of intertidal invertebrates in the northeast Pacific Ocean. *Ecology,* **82,** 1799–1813.

Cutchin, D. L., and R. L. Smith, 1973: Continental shelf waves: Low-frequency variations in sea level and currents over the Oregon continental shelf. *J. Phys. Oceanogr.,* **3,** 73–82.

Federiuk, J., and J. S. Allen, 1995: Upwelling circulation on the Oregon continental shelf. Part II: Simulations and comparisons with observations. *J. Phys. Oceanogr.,* **25,** 1867–1889.

Gan, J., and J. S. Allen, 2002: A modeling study of shelf circulation off northern California in the region of the Coastal Ocean Dynamics Experiment: Response to relaxation of upwelling winds. *J. Geophys. Res.,* **107,** 3123, doi:10.1029/2000JC000768.

——, and ——, 2005: Modeling upwelling circulation off the Oregon coast. *J. Geophys. Res.,* **110,** C10S07, doi:10.1029/2004JC002692.

Gordon, R. L., 1996: Acoustic Doppler Current Profiler: Principles of operation: A practical primer. 2nd ed. Broadband ADCPs, RD Instruments, 54 pp.

Huyer, A., 1983: Coastal upwelling in the California Current System. *Prog. Oceanogr.,* **12,** 259–284.

——, R. L. Smith, and R. D. Pillsbury, 1974: Observations in a coastal upwelling region during a period of variable winds (Oregon coast, July, 1972). *Tethys,* **6,** 391–404.

——, B. M. Hickey, J. D. Smith, R. L. Smith, and R. D. Pillsbury, 1975: Alongshore coherence at low frequencies in currents observed over the continental shelf off Oregon and Washington. *J. Geophys. Res.,* **80** (C24), 3495–3505.

Kirincich, A. R., J. A. Barth, B. A. Grantham, B. A. Menge, and J. Lubchenco, 2005: Wind-driven inner-shelf circulation off central Oregon during summer. *J. Geophys. Res.,* **110,** C10S03, doi:10.1029/2004JC002611.

Kosro, P. M., 2005: On the spatial structure of coastal circulation off Newport, Oregon, during spring and summer 2001 in a region of varying shelf width. *J. Geophys. Res.,* **110,** C10S06, doi:10.1029/2004JC002769.

Kuebel Cervantes, B. T., J. S. Allen, and R. M. Samelson, 2003: A modeling study of Eulerian and Lagrangian aspects of shelf circulation off Duck, North Carolina. *J. Phys. Oceanogr.,* **33,** 2070–2092.

Kundu, P. K., and J. S. Allen, 1976: Some three-dimensional characteristics of low-frequency current fluctuations near the Oregon coast. *J. Phys. Oceanogr.,* **6,** 181–199.

——, ——, and R. L. Smith, 1975: Modal decomposition of the velocity field near the Oregon coast. *J. Phys. Oceanogr.,* **5,** 683–704.

Large, W. G., and S. Pond, 1981: Open ocean momentum flux measurements in moderate to strong winds. *J. Phys. Oceanogr.,* **11,** 324–336.

Lentz, S. J., 1994: Current dynamics over the northern California inner shelf. *J. Phys. Oceanogr.,* **24,** 2461–2478.

——, and C. D. Winant, 1986: Subinertial currents on the southern California shelf. *J. Phys. Oceanogr.,* **16,** 1737–1750.

——, and D. C. Chapman, 2004: The importance of nonlinear cross-shelf momentum flux during wind-driven coastal upwelling. *J. Phys. Oceanogr.,* **34,** 2444–2457.

——, R. T. Guza, S. Elgar, F. Feddersen, and T. H. C. Herbers, 1999: Momentum balances on the North Carolina inner shelf. *J. Geophys. Res.,* **104,** 18 205–18 226.

Leslie, H. M., E. N. Breck, F. Chan, J. Lubchenco, and B. A. Menge, 2005: Barnacle reproductive hotspots linked to nearshore ocean conditions. *Proc. Natl. Acad. Sci. USA,* **102,** 10 534–10 539.

Liu, Y., and R. H. Weisberg, 2005: Momentum balance diagnoses for the West Florida shelf. *Cont. Shelf Res.,* **25,** 2054–2074.

Menge, B. A., E. Sanford, B. A. Daley, T. L. Freidenburg, G. Hudson, and J. Lubchenco, 2002: An inter-hemispheric comparison of bottom-up effects on community structure: Insights revealed using the comparative-experimental approach. *Ecol. Res.,* **17,** 1–16.

Munchow, A., and R. Chant, 2000: Kinematics of inner shelf motions during the summer stratified season off New Jersey. *J. Phys. Oceanogr.,* **30,** 247–268.

Oke, P. R., J. S. Allen, R. N. Miller, and G. D. Egbert, 2002: A modeling study of the three-dimensional continental shelf circulation off Oregon. Part II: Dynamical analysis. *J. Phys. Oceanogr.,* **32,** 1383–1403.

Pawlowicz, R., B. Beardsley, and S. Lentz, 2002: Classical tidal harmonic analysis including error estimates in MATLAB using T_TIDE. *Comput. Geosci.,* **28,** 929–937.

Perlin, A., J. N. Moum, J. M. Klymak, M. D. Levine, T. Boyd, and P. M. Kosro, 2005: A modified law-of-the-wall applied to oceanic bottom boundary layers. *J. Geophys. Res.,* **110,** C10S10, doi:10.1029/2004JC002310.

Pierce, S. P., J. A. Barth, R. E. Thomas, and G. W. Fleischer, 2006: Anomalously warm July 2007 in the northern California Current: Historical context and significance of cumulative wind stress. *Geophys. Res. Lett.,* **33,** L22S04, doi:10.1029/2006GL027149.

Samelson, R., and Coauthors, 2002: Wind stress forcing of the Oregon coastal ocean during the 1999 upwelling season. *J. Geophys. Res.,* **107,** 3034, doi:10.1029/2001JC000900.

Smith, R. L., 1974: A description of current, wind, and sea level variations during coastal upwelling off the Oregon coast, July–August 1972. *J. Geophys. Res.,* **79,** 435–443.

Tilburg, C. E., 2003: Across-shelf transport on a continental shelf: Do across-shelf winds matter? *J. Phys. Oceanogr.,* **33,** 2675–2688.

——, and R. W. Garvine, 2003: Three-dimensional flow in a shallow coastal upwelling zone: Alongshore convergence and divergence on the New Jersey shelf. *J. Phys. Oceanogr.,* **33,** 2113–2125.

Wiseman, W. J., and R. W. Garvine, 1995: Plumes and coastal currents near large river mouths. *Estuaries,* **18,** 509–517.

Yankovsky, A. E., and D. C. Chapman, 1995: Generation of mesoscale flows over the shelf and slope by shelf wave scattering in the presence of a stable, sheared mean current. *J. Geophys. Res.,* **100** (C4), 6725–6742.

——, R. W. Garvine, and A. Münchow, 2000: Mesoscale currents on the inner New Jersey shelf driven by the interaction of buoyancy and wind forcing. *J. Phys. Oceanogr.,* **30,** 2214–2230.